Tectonophysics 817 (2021) 229048

Contents lists available at ScienceDirect

Tectonophysics

journal homepage: www.elsevier.com/locate/tecto

Seismicity patterns along the northern Manila Trench reflect crustal properties of the subducting plate☆

Jing-Yi Lin [a,b,*], Yi-Ching Yeh [a], Sin-Mei Ng [c], An Li [a], Shao-Jinn Chin [d], Yi-Chin Lin [a], Chin-Wei Liang [b]

[a] Department of Earth Sciences, National Central University, Taoyuan 32001, Taiwan
[b] Center for Environmental Studies, National Central University, Taoyuan 32001, Taiwan
[c] Department of Geology, Chinese Culture University, Taipei 11114, Taiwan
[d] School of Geography, Environment and Earth Sciences, Victoria University of Wellington, Wellington 6140, New Zealand

ARTICLE INFO

Keywords:
Manila Trench
South China Sea
Luzon Ryukyu transform plate boundary
Ocean bottom seismometer
Outer rise earthquakes
Continental-ocean boundary
Crustal thickness
Seismogenic structure

ABSTRACT

We examine the seismicity recorded by two temporary ocean bottom seismometer arrays deployed along the northeastern Manila Trench, covering the outer rise and part of the accretionary wedge. A total of 1437 events were determined during the 44-day recording period, showing a relatively more dynamic seismic activity than previously thought. Most events occurred in the subducting plate, oceanward of the trench, at depths between 25 and 50 km and revealed normal-fault type mechanisms. The relatively deeper focal depth and the lack of well-developed outer rise bulge near the seismic cluster suggest an untypical pattern of outer rise earthquakes. Seismicity with a high occurrence frequency and small magnitude is typical of earthquakes swarm, which is generally thought to be driven by fluid pressure variations. We suggest the infiltration of seawater through fractures into the rifted South China Sea margin is the main driver of the earthquakes detected during our deployments. Because earthquakes are also more abundant in the area where a significant change of crustal thickness is documented, we suggest the inherited crustal properties and tectonic structures strongly control the seismic behavior along the Manila subduction system.

1. Introduction

Located in the Western Pacific Ocean, the South China Sea (SCS) is a rifted passive margin. The almost N-S trending Manila subduction system forms the northeastern boundary of the SCS, where the Eurasian plate is actively subducting eastward underneath the Philippine Sea plate. This structure is terminated to the north by the Taiwan collision zone, and to the south by the Sulu-Palawan block. The relative motion of Philippine Sea plate is estimated to be between 7 and 8.2 cm/yr relative to Eurasian plate revealed by the plate reconstruction (Seno et al., 1993) and the geodetic analyses (Hsu et al., 2009; Yu et al., 1997). Convergence rate along the subduction system have been estimated to be more than 50 mm/yr near Taiwan, 100 mm/yr near the northern Luzon Island, and 50 mm/yr to the southernmost end of the trench (Galgana et al., 2007; Rangin et al., 1999). The high convergence rate, together with the discovery of a possible splay faults in the Manila accretionary wedge, make the Manila Trench the most hazardous tsunami source in South China Sea (Lin et al., 2009; Qiu et al., 2019). Numerous scenarios have been discussed about the impact of a possible tsunami in this area (Qiu et al., 2019; Wu et al., 2009). However, based on seismological data, gravity simulation and gravity potential energy estimation, several studies have proposed that certain parts of the Manila Trench system are weakly coupled (Chin et al., 2019; Doo et al., 2015; Lin et al., 2015; Lo et al., 2017; Tan, 2020). In addition, in contrast with the rapid strain rate distribution, only a few moderate to large earthquakes were recorded in the past decades (Wu et al., 2010). The Pingtung doublet earthquakes (26 December 2006) are the most recent and the largest seismic events recorded off SW Taiwan. Based on the regional tomographic result, the source area of the two M_L 7.0 earthquakes was suggested to be in and/or beneath the subducted slab rather than along the plate interface (Liao et al., 2008). It is proposed that these earthquakes are the result of the deflection of the east-dipping Eurasian plate caused by Taiwan orogenic load.

The SCS seafloor was characterized by numerous ancient crustal

☆ Submitted to Special Issue Tectonophysics Geodynamics and Extreme Events in Taiwan and South-East Asia Geet-Sea

* Corresponding author at: Department of Earth Sciences, National Central University, Taoyuan 32001, Taiwan.
E-mail address: jylin@ncu.edu.tw (J.-Y. Lin).

https://doi.org/10.1016/j.tecto.2021.229048
Received 31 March 2021; Received in revised form 10 August 2021; Accepted 29 August 2021
Available online 8 September 2021

structures, such as seamount and fracture zones. The presence of oceanic crust was firstly defined with magnetic lineation. However, between the continent and the oceanic plate, the transitional crust usually lacks clear magnetic anomaly. The boundary of the continent-ocean transition and normal oceanic crust is called the continent-ocean boundary (COB). Briais et al. (1993) suggested that the COB intersects the Manila Trench at 19°N based on the seafloor magnetic anomaly distribution (Fig. 1). Based on the *E*-W trending magnetic lineation offshore southwestern Taiwan, Hsu et al. (2004) rather suggested that the northern SCS crust is entirely oceanic to 21.5°N. The rapid thinning of the continental crust from the continental shelf to the ocean has been imaged in the northeastern SCS based on geophysical investigations (Eakin et al., 2014; Lester et al., 2014; Lester et al., 2013; Tsai et al., 2004; Wang et al., 2006; Yeh et al., 2012). Between the continental crust and the normal oceanic crust, an extended continental crust with a thickness of 11–15 km as far south as 20°N has been reported, delineated the approximate location of COB (Eakin et al., 2014; McIntosh et al., 2013) (Fig. 1a). While the COB position is debated, the evaluation of the crustal thickness of the SCS between 20°N and 21°N appears to be consistent (Eakin et al., 2014; Yeh et al., 2012).

The Luzon–Ryukyu transform plate boundary (LRTPB) is also a prominent morphotectonic feature in the northeastern SCS (Fig. 1). Sibuet et al. (2002) has interpreted this structure as a former left-lateral transform fault, connecting the former northwest-dipping Ryukyu Trench in the northwest and the former southeast-dipping Manila Trench in the southeast. The LRTPB is suggested to have ceased activity since ~20 Ma (Hsu et al., 2004). A relatively thin crust, revealed by gravity modelling, can be observed beneath the LRTPB, demonstrating the LRTPB corresponds to a shear zone (Yeh and Hsu, 2004). However, the transtensional deformation is observed only near the northwest and southeast ends of the LRTPB (Yeh et al., 2012). This phenomenon is probably due to presence of post-spreading magmatism imprinting on the pre-existing SCS crust (Hsu et al., 2004). The two sides of LRTPB are characterized by slightly different crustal thickness with a thicker oceanic crust to the west (McIntosh et al., 2013; Yeh et al., 2012).

The subduction of all the above-mentioned seafloor edifices could have significant impact on the deformation as suggested by the various type of focal mechanisms observed in the area (e.g. Lin et al., 2015; Chin et al., 2019; Wu et al., 2021)(Fig. 1b). The inherited regional structures and tectonic process could affect the seismogenic behavior of subduction zone and therefore have direct impact on the assessment of seismic hazard (e.g. Lallemand et al., 2018). To improve our understanding of the interactions of all these marine structures with the trench and/or the related seismic hazard of the Manila subduction zone, geophysical investigations have also been conducted. Even though several crustal and/or lithospheric-scale features have been illustrated, it is still unclear how these structures affect the subduction process. In this paper, we present results from the deployment of two temporary ocean bottom seismometer arrays along the northeastern Manila Trench, covering the outer rise and part of the accretionary wedge. The earthquakes distribution inferred from our deployment is then compared to the regional tectonic structures and the Global Centroid Moment Tensor (GCMT) catalog

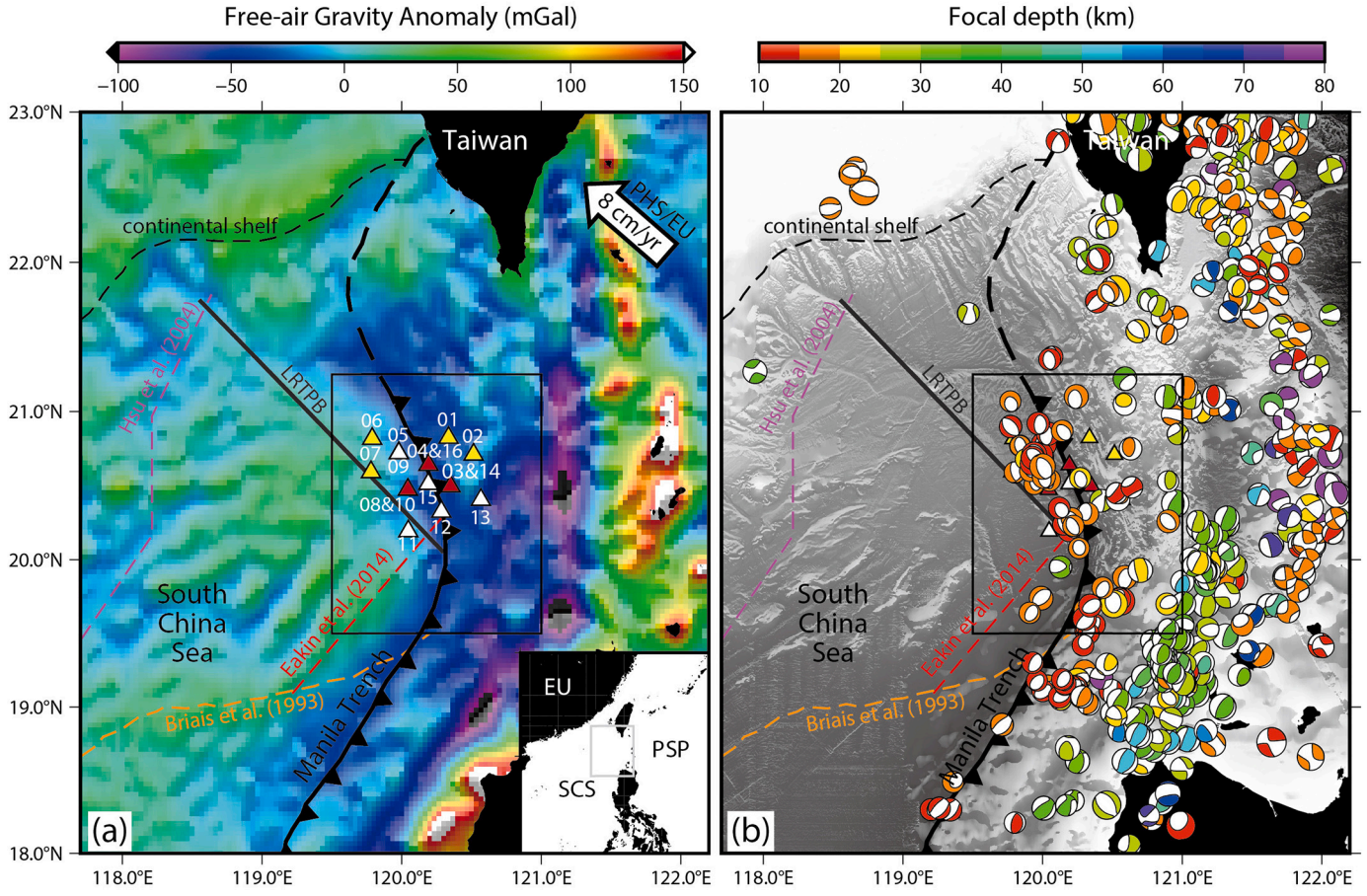

Fig. 1. Free-air gravity anomaly map (a) and Global Centroid Moment Tensor(GCMT) catalog focal mechanisms from 1976/01/01 to 2021/06/30 (b) of the northern-most South China Sea. Triangles show the position of ocean bottom seismometers. Yellow and white triangles are the OBSs deployed in 2016 and 2017. Red triangles are the overlapped OBSs, which means the OBS is deployed in the same position both in 2016 and 2017. Orange, purple and red dashed line represents the continent-ocean boundary (COB) determined by Briais et al. (1993), Hsu et al. (2004) and Eakin et al. (2014), respectively. Black line shows the Luzon-Ryukyu Transition Plate Boundary (LRTPB). PSP: Philippine Sea Plate; SCS: South China Sea. The black rectangle shows the position of Figs. 2 and 5. (For interpretation of the references to colour in this figure legend, the reader is referred to the web version of this article.)

along the northeastern Manila subduction system. This is then used to evaluate the tsumani and shaking hazards in the Southeast Asia area.

2. Data and processing

We have deployed two temporary ocean bottom seismometer (OBS) arrays designed to investigate the distribution of global seismicity distribution along the Manila Trench (Fig. 1a). The study area is about 90 km × 50 km, covering the outer rise and part of the accretionary wedge (Table 1). Both networks consist of 8 OBSs and deployed from June 22 to July 12, 2016 and from June 27 to July 20, 2017, respectively. The survey areas of the two networks are overlapping (stations marked in red in Table 1 and red triangles in Fig. 1) in order to monitor the time-dependent variation of the seismic activities in our studied area. For example, the position of OBS03 deployed in 2016 and OBS14 deployed in 2017 is almost identical (Table 1). The instruments used in the two operations were developed by the French Research Institute for Exploitation of the Sea (Ifremer) (Auffret et al., 2004). Each MicrOBS contains one hydrophone and three orthogonal 4.5 Hz geophones and record data with a sampling rate of 125 Hz. A preliminary examination for possible events was performed by using the STA/LTA algorithm (Trnkoczy, 2009), which detects the changes in the amplitude at several stations. Then, we manually inspect the arrivals, assigning a subjective weight. In total, 1437 locatable events, containing 7376 P- and 7253 S-wave arrivals, were successfully localized using the global IASP91velocity model (Kennett and Engdahl, 1991) during the 44-day recording period, that is approximately 30 events per day (Fig. 2a). Due to the complex structure setting in our study area, the use of 1-D velocity model must not be sufficient. Thus, the SIMUL2000 method (Thurber, 1983), which allows the inversion of a 3-D velocity model from the dataset and a relocation of events, was applied to obtain a more rational result. While applying the SIMUL2000 software, we use the 1-D velocity model estimated based on seismic refraction data (Eakin et al., 2014) as initial model. The grid space is 10 km horizontally and 5 km vertically. The damping values were decided by the trade-off curve between the data variance and model variance (Fig. 3), and the final applied value is 10. After applying SIMUL2000, several events with large residual have been removed from the GCMT catalog and 1210 events were finally relocated (Fig. 2b). Antelope software magnitude calculator DBEVPROC, which uses the largest amplitude of the three-component instrument-response-corrected seismograms is applied to estimate the magnitude of each event.

Table 1
Station information. OBS01 to OBS08 are deployed in 2016. OBS09 and OBS16 are deployed in 2017. Stations in red colour indicate the overlapped stations. OBS03 and OBS 14, OBS04 and OBS 16, OBS 08 and OBS10 are at same position.

Name of station	Longitude (°E)	Latitutde (°N)	Depth (m)
OBS01	120.336	20.824	2790.2
OBS02	120.515	20.711	2410.3
OBS03	120.350	20.496	3678.2
OBS04	120.192	20.641	3743.8
OBS05	119.979	20.721	3615.0
OBS06	119.789	20.816	3275.8
OBS07	119.780	20.592	3170.8
OBS08	120.044	20.474	3506.3
OBS09	119.980	20.720	3611.7
OBS10	120.003	20.440	3468.7
OBS11	120.047	20.193	3525.3
OBS12	120.284	20.325	3998.3
OBS13	120.567	20.405	3418.1
OBS14	120.350	20.496	3685.9
OBS15	120.190	20.513	3870.6
OBS16	120.192	20.642	3745.1

3. Results and discussion

3.1. Hypocenters determination using different velocity models

The tectonically complex subduction system is characterized by large heterogeneity in the seismic velocities distribution, which usually cause problems while performing earthquakes relocation. In our study, the earthquakes were located initially by using IASP91 global velocity model, then relocated with SIMUL 2000 software. To further examine the spatial variation of earthquakes distribution, we calculated the hypocenter displacement before and after the relocation which is estimated to be about 5 to 7 km as shown in Fig. 4. We do also find an average downward migration of focal depths of 5 to 10 km in the vertical component (Z axis), while only a relatively smaller eastward migration (about 4 to 6 km) occurs in the horizontal component (XY axis) (Fig. 4). Despite the decrease of the number of earthquake after the relocation, the earthquakes distribution map displays similar pattern (Fig. 2). The deepening of hypocenters after relocation is particularly obvious for the earthquakes located to the west of the trench. For earthquakes occurring in this area, the focal depth is about 20 to 30 km initially, while it becomes deeper than 30 km after relocation. In contrast, the seismic cluster located landward of the trench keeps similar depth range after the relocation. This systematic deepening of hypocenters for the earthquakes located to the west of the trench should be due to the use of a larger velocity for the relocation. The average value of the IASP91 model at 35 km is 6.15 km/s, a worldwide average for crustal velocity. However, the velocity model used for the earthquakes relocation is based on Eakin et al. (2014), in which the crust thickness is estimated to be about 9–15 km, indicating an hyper-extended continental crust or an oceanic crust. When the depth is deeper than the bottom of the oceanic crust, a velocity of higher than 7.5 km/s was used. Thus, the average velocity applied for the relocation should be much faster than the one used for the initial relocation (i.e. IASP 91). For identical travel time, when the velocity increases, the focal depth must deepen. On the other hand, as the velocity structure of Eakin et al. (2014) to the east of the trench is close to that of IASP91 model, the vertical displacement of earthquakes is minimum (Fig. 2). In terms of horizontal variations, an eastward displacement of relocated earthquakes is observed mostly for the earthquakes located to the east of the trench (Fig. 2). This likely reflect the different velocity structures on the two sides of the Manila Trench. Since the seismic velocity becomes faster to the western side of the trench, the earthquakes located to the east of the seismic network move further to the east for a fixed travel time.

We infer that the changes in the velocity model do not result in significant changes in the horizontal direction, while variations in vertical direction are notable. In other words, the epicenters of earthquakes seem not largely affected by the use of different velocity models, which means that our results are robust. However, the faster the velocity used in the model, the deeper the hypocenters. As the velocity used in the relocation is obtained from in-situ geophysical investigation (Eakin et al., 2014), the focal depth should be more reliable after relocation. Even though the depth of the earthquakes determined in our study appears larger than general thought (e.g. Chang et al., 2012), it is worth noting that the earthquakes could not be much shallower unless a crustal velocity of 3 km/s is used for the earthquakes localization, which is not rational in our study area.

3.2. Seismicity distribution and inherited lower plate structures

A total of 1437 events have been determined during the 44-day recording period, that is approximately 30 events per day. Most earthquakes have a magnitude smaller than 3 (Fig. 5). During that period, no earthquakes were recorded in the GCMT catalog. The earthquake distribution shows that most events occurred within the subducting plate below the Moho at depths between 25 and 50 km and oceanward of the trench (Figs. 2 and 5). This earthquakes group seems to align along a

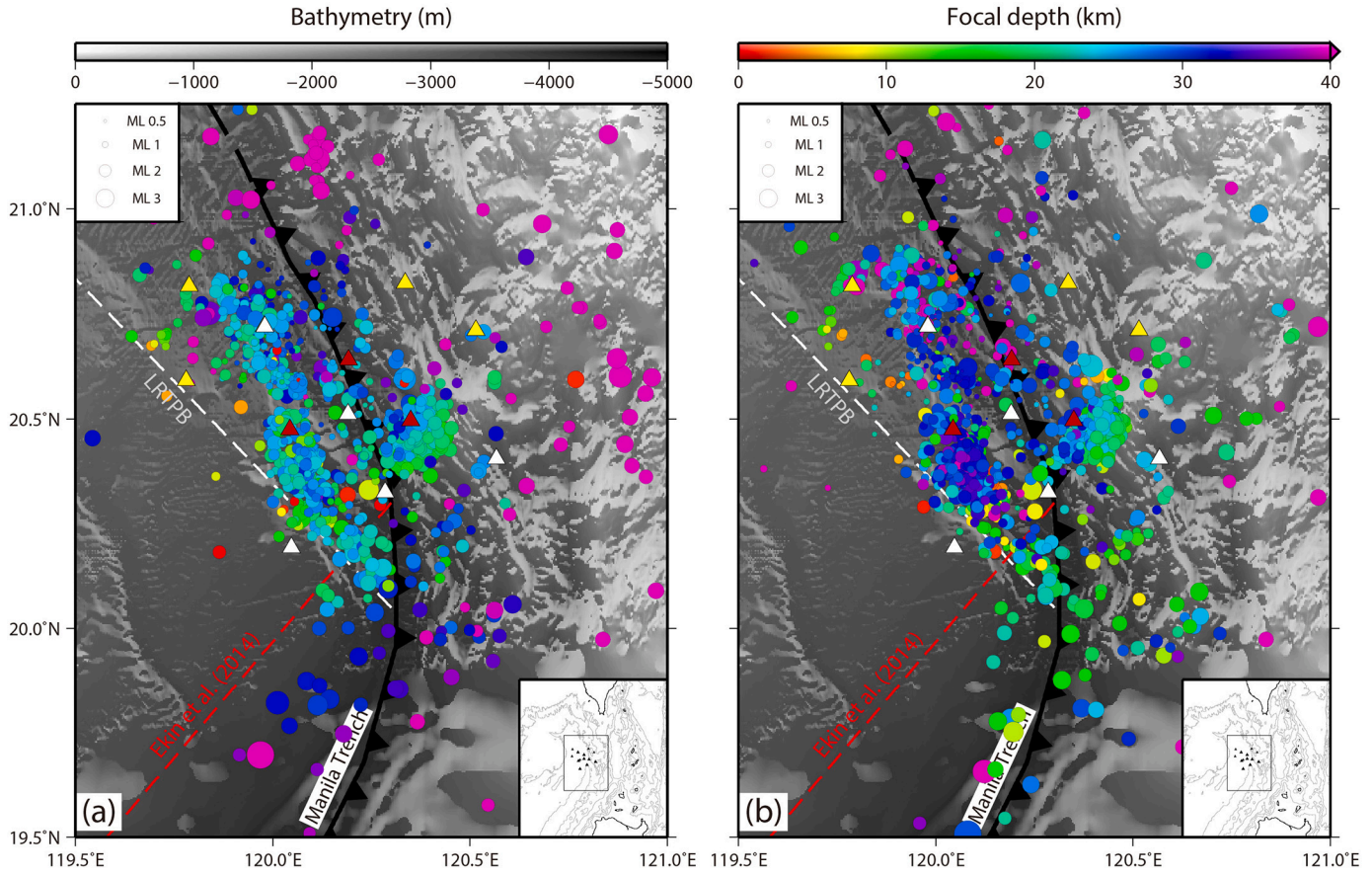

Fig. 2. Earthquakes distribution in map view. (a) and (b) are the hypocenters located by using IASP91 velocity model and SIMUL 2000 software. Triangles show the position of ocean bottom seismometers. White and red dashed line represents LRTPB and the COB determined by Eakin et al. (2014). Dots show the earthquakes determined in our study. The size and the colour of the dots indicate the magnitude and the focal depth of the event. (For interpretation of the references to colour in this figure legend, the reader is referred to the web version of this article.)

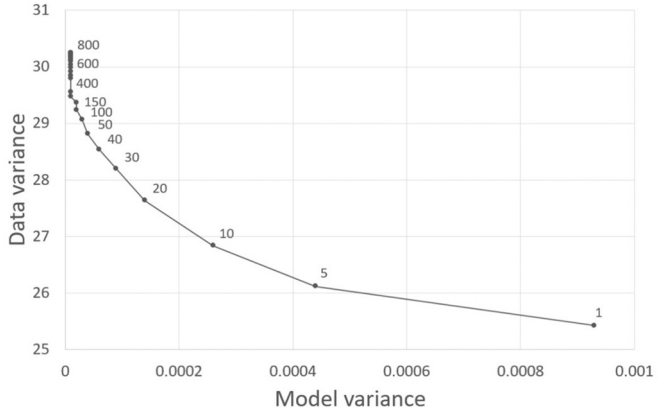

Fig. 3. Trade off curve of the data variance and model variance while applying SIMUL 2000 software for earthquakes relocalization.

NW-SE trending structure. The hypocenters distribution along sections striking NW-SE (BB'), NE-SW (AA' and CC') (Figs. 5 and 6) shows a slightly southward and eastward-dipping features, which corresponds to the subducting Eurasian plate. Along AA' profile, the seismic activity clustering at about 26 km and appears limited to the southwest by the LRTPB. This cluster of earthquakes stops at 80 km along the BB' profile (approximately 22.2°N in map view), where both the COB determined by Eakin et al. (2014) and LRTPB intersect the Manila Trench. Close to this boundary, a relatively higher density of events is observed. The magnitude of earthquakes is also larger (Figs. 5 and 6b), with magnitudes above 3, whereas most events to its northern and southern part have a magnitude smaller than 2 (Fig. 5). LRTPB was suggested to be an important tectonic feature, which plays a role as a former left-lateral transform fault (Hsu et al., 2004; Sibuet et al., 2002). We find that almost all the earthquakes are located oceanward side of the trench and are enclosed in the area stretching between the LRTPB and the trench. Note that this spatial distribution of earthquakes is well constrained by two OBSs deployed across the LRTPB (OBS07 and OBS11 in Fig. 1a). The location of this earthquake cluster is in a good agreement with the focal mechanisms distribution reported by the global GCMT catalog, which shows a concentration of seismicity with normal faulting mechanism parallel to the trench (Fig. 1b). This trench-parallel distribution of earthquakes is generally considered to occur on the outer rise area of a subduction system (Chang et al., 2012), as a result of the bending of the downgoing lithosphere.

Landward of the trench, the earthquakes seem to concentrate at one position, which is about 120.45°E; 20.45°N, near OBS 14. Those earthquakes show no distinct pattern both on map and cross-section (Figs. 5 and 6a). While examining the waveform data, we found that many events can only be recognized on OBS 14 and cannot be located successfully. This earthquake cluster coincides with the northeastern prolongation of the COB determined from the crustal thickness variation and velocity distribution (Eakin et al., 2014) (Fig. 2b). However, since the position of the COB is still highly debatable, we describe this boundary as a zone where the crustal thickness decreases rapidly from about 12 km to 8 km toward the south (Yeh et al., 2012). Such lateral variations of crustal thickness in the subduction zone may play a role in

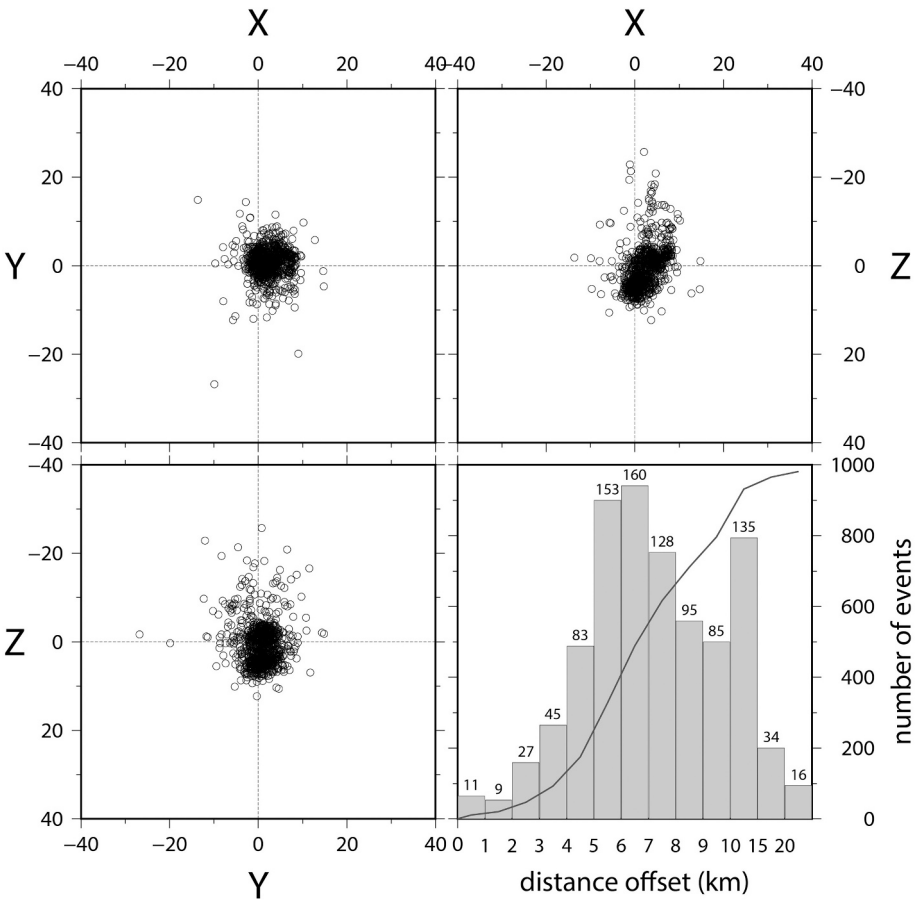

Fig. 4. Spatial variation of earthquakes distribution after relocation is shown in (a) to (c). Positive value indicates deepening for the Z axis; eastward migration for the X axis and southward migration for Y axis. The offset after the relocation v.s. the number of events is shown in (d).

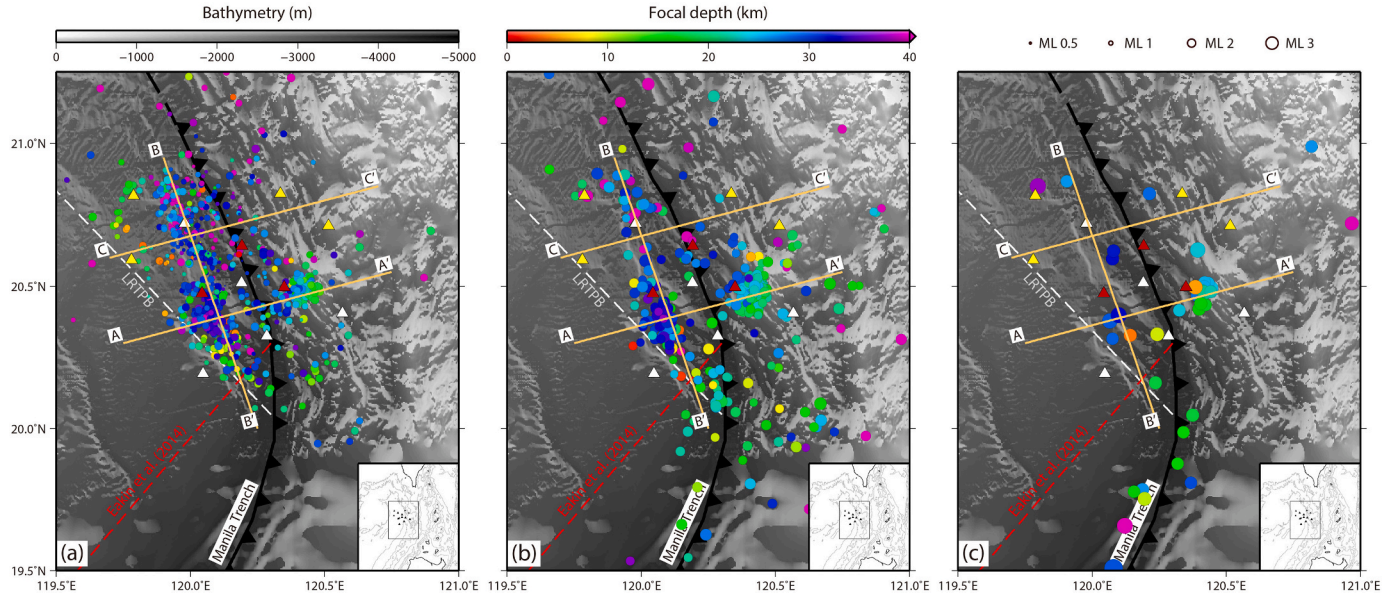

Fig. 5. Mapview of the earthquakes for different magnitude ranges. (a), (b) and (c) show the events with magnitude less than 2, between 2 and 3, and larger than 3, respectively. Orange lines indicate the position the three cross-section AA', BB' and CC'. Other figure caption is the same as in Fig. 2.

the generation of earthquake clusters.

3.3. Seismogenic characteristics of the area

As indicated in the previous section, two major groups of earthquakes are recognized. One group of earthquakes is located oceanward

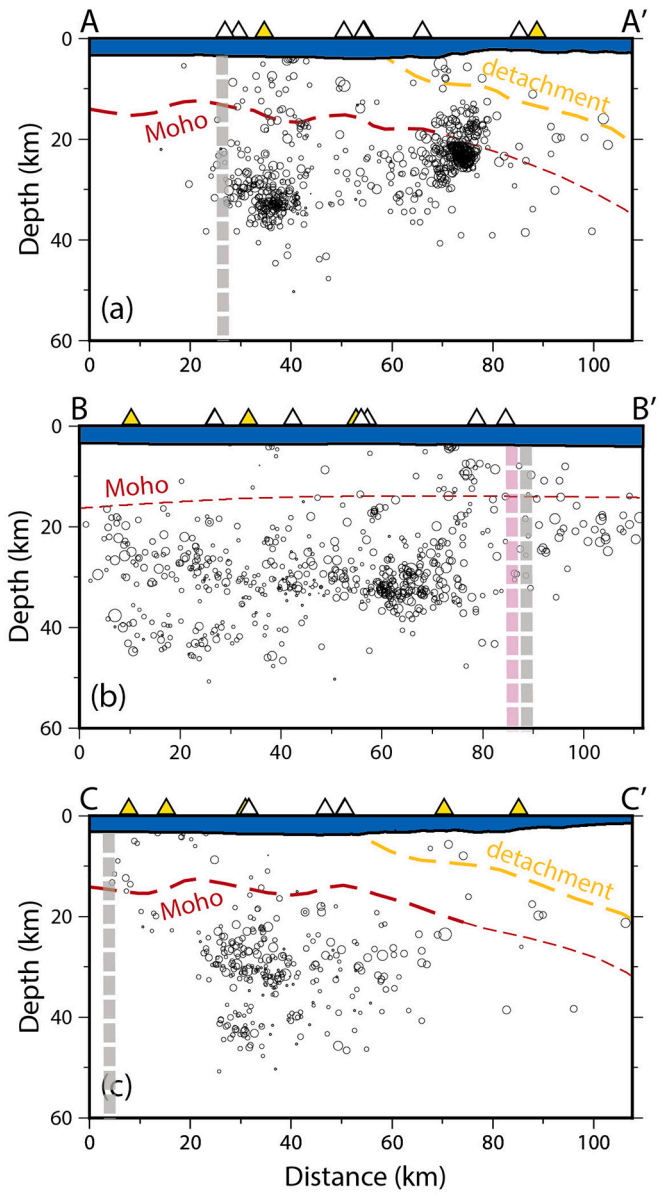

Fig. 6. Earthquakes distribution along AA', BB' and CC' cross-section. The earthquakes (dots) located within 20 km and the seismic stations (triangles) located within 25 km of the cross section are projected. The position of the three profiles is shown in Fig. 5. The position of "detachment" (orange dashed line) and "Moho" (red dashed line) has been extracted and modified from Eakin et al. (2014) and Yeh et al. (2012). Gray and pink bold dashed line are the position of the COB determined from Eakin et al. (2014) and LRTPB. (For interpretation of the references to colour in this figure legend, the reader is referred to the web version of this article.)

of the trench near the outer rise, between the LRTPB and the Manila Trench and show an approximately trench-parallel distribution pattern. Earthquakes reported in the crust and mantle at the outer rise of some subduction systems are thought be caused by flexural bending and mantle serpentinization of the oceanic lithosphere. Modelling of the extensional stress in the outer rise area show that outer rise earthquakes occur principally in the upper half of the down-bending plate and their focal depths are generally shallower than 30 km (Christensen and Ruff, 1988; Craig et al., 2014). However, most of the earthquakes determined from our study, as well as from the global earthquake catalog, occurred at depth deeper than 30 km. Based on numerical thermo-mechanical modelling, Tan (2020) have demonstrated that the deep normal fault earthquakes observed along the Manila Trench can be explained by the subduction of a transitional crust. Our study area located to the north of the COB is made of a thinned continental crust with crustal thickness ranging between 12 and 15 km (Eakin et al., 2014; Yeh et al., 2012) (Figs. 1, 6 and 7). Based on the seismic reflection data, numerous normal faults have been determined in the northeastern portion of SCS. Most of these faults cut through the upper crust and some of them affect the Moho (Ku and Hsu, 2009; Lester et al., 2013; McIntosh et al., 2013; Yeh and Hsu, 2004; Yeh et al., 2012). The crust in the area between the LRTPB and the Manila Trench has been recognized as highly fractured (Ku and Hsu, 2009; Yeh and Hsu, 2004). For example, the yellow segments in Fig. 7 determined from seismic reflection profiles (Yeh and Hsu, 2004) illustrate crustal scale normal faults that defined a rugged bathymetry. The low free-air gravity anomaly is at odds with the positive gravity anomaly signature expected in the forebulge area (e.g. Watts and Talwani, 1974)(Fig. 1). We hypothesize that this highly faulted domains and the low gravity anomaly could be linked to the nature of the thinned continental crust. Such highly deformed lithospheric characteristics could result from the pre-existing normal faults created during the SCS rifting in addition to the newly formed faults caused by ongoing subduction. Most of the earthquakes determined in our study area formed in the weak thinned continental margin located between LRTPB and the trench, with a depth deeper than the Moho (red dots in Fig. 7). The great depths of the earthquakes suggest that there is less possibility to be generated directly by the reactivation of pre-existing normal faults or any other newly form crustal structures. The stress or strain concentration linked to the highly heterogeneous crust properties appears to be the main mechanism which drives the main deformation pattern in the area. Furthermore, the earthquakes are generally characterized by small magnitude and a high frequency of occurrence (high b value, repeated occurrence), which is typical of swarm activity. Based on empirical evidence and theoretical considerations, this seismicity feature is generally thought to be driven by the alteration of fluid pressure (Tilmann et al., 2008; Yamashita, 1999). The hydration of the plate down to the depths of several tens of kilometers have been discussed by quite a few observational and theoretical studies (e.g., Peacock, 2001; Grevemeyer et al., 2007; van Avendonk et al., 2011; Naif et al., 2015). Result shows that thermal cracking and bending-related faulting could be sufficient to explain the existence of small crack-like porosities at deep depth, which could increase the water content in the mantle part (Korenaga, 2017). Therefore, we suggest that the seawater may enters to the Moho through the large-scale normal faults and cause the swarm activity at deeper depth (black arrows in Fig. 7). Similar observation and mechanism have also been suggested for the Chile and Cascadia subduction areas (Contreras-Reyes et al., 2007; Ivandic et al., 2010; van Avendonk et al., 2011; Tilmann et al., 2008). Finally, the presence of the LRTPB (white bold dashed line in Fig. 7) seems to be a major boundary that effectively limit the earthquakes distribution to its east. Even though this tectonic feature is no longer active (Hsu et al., 2004; Yeh et al., 2010), it may still affect the stress propagating state. Another possibility is that the crustal materials on the two sides of the LRTPB may be different originally which causes distinct seismogenic behavior on its two sides.

The other area with distinct seismic activity is located landward of the trench, specifically at about 120.45°E; 20.45°N. Previous description has indicated a good agreement between the location of this earthquake cluster and the domains characterized by the abrupt change in crustal thickness (i.e. COB determined by Eakin et al. (2014) in Fig. 7). We suggest that the subduction of lithosphere with different crustal thickness may induce some stress variation along the boundary and generate earthquakes. However, the earthquake cluster has similar characters as the seismic cluster located in the oceanward of the trench, which is the occurrence of earthquakes have a high repeatability with relatively small magnitude. Thus, the presence of fluid may also be an important factor affecting the seismogentic behavior in this area (Becker et al., 2006).

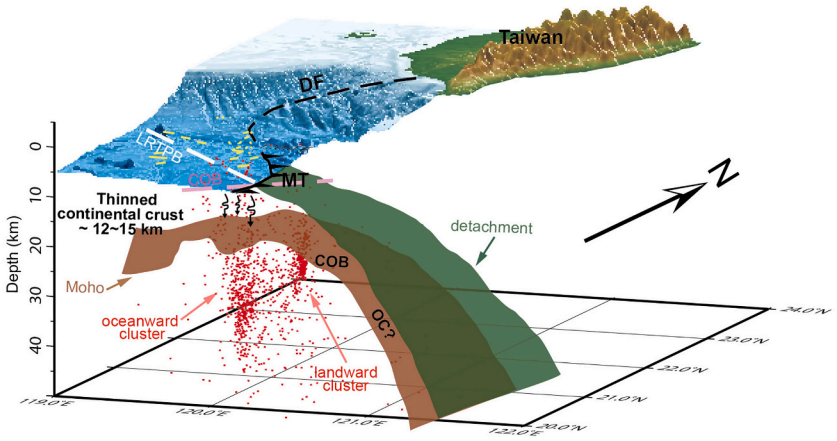

Fig. 7. Diagram showing the seismogenic environment of the northern Manila Trench system, in the north-eastern corner of the South China Sea area. The "detachment" and "Moho" are extracted based on the seismic refraction profiles data along 20.5°N and 21.4°N in Eakin et al. (2014). The yellow segments on the seafloor indicate the position of normal faults determined by Yeh and Hsu (2004). White and pink dashed line represents LRTPB and the COB determined by Eakin et al. (2014). Red dots show the earthquakes. Black arrows indicate seawater penetration, which was suggested to be the origin of the seismicity at great depth with small magnitude and high repeatability. MT: Manila Trench; OC: oceanic crust. Our area is almost located to the north of the COB, which is suggested to be a thinned continental crust. (For interpretation of the references to colour in this figure legend, the reader is referred to the web version of this article.)

4. Conclusions

We have examined the seismicity recorded by two temporary ocean bottom seismometer arrays deployed along the northeastern Manila Trench, covering the outer rise and part of the accretionary wedge. Earthquakes distribution shows that a large portion of recorded events occurred in the subducting plate, oceanward of the trench, at depths between 25 and 50 km. Even though the earthquakes are located close to the outer rise of the trench and show approximately trench-parallel pattern, the low free-air gravity anomaly show inconsistency with the typical outer rise properties. In addition, the remarkable exception of deep normal fault earthquakes in the area does not conform to the concept about the depth range of the outer rise events. Earthquakes with great focal depths observed near the seismic cluster reveals untypical outer rise earthquakes. Most events were characterized by a magnitude smaller than 3 with only 4% of them with a magnitude larger than 3. The high occurrence frequency and small magnitude of earthquakes suggest a swarm-type activity, which is generally thought to be driven by fluid pressure variations. We consider the penetration of seawater through fractures in the highly fragmented rifted continental crust could be the origin. As the normal faults created by the opening of SCS or/and the ongoing subduction cut through the crust and reach the Moho as already evidenced by many previous studies, fluid may reach Moho and cause earthquakes at that depth. Moreover, the change of the lithosphere nature are thought to affect the seismogenic attitude. The fact that earthquakes are located in a thinned continental margin where crustal thickness vary and that they are closely related to the position of a lithospheric feature (LRTPB) suggest that the inherited tectonic structures and crustal properties could control the stress distribution along the Manila trench. The stress or strain concentration linked to the highly heterogeneous crust properties could be also a main mechanism which drives the deformation pattern in the area.

Declaration of Competing Interest

The authors declare that they have no known competing financial interests or personal relationships that could have appeared to influence the work reported in this paper.

Acknowledgements

The authors acknowledge the two anonymous reviewers who provided thorough feedback that greatly improved the manuscripts. Special thanks to the guest editor Professor Frederic Mouthereau for the pertinent and relevant remarks with regard to our interpretation. All figures were made by the Generic Mapping Tools (Wessel and Smith, 1998). This research was supported by the Central Weather Bureau of Taiwan with grant MOTC-CWB-108-E-05 and by the Ministry of Science and Technology, Taiwan, under contract 107-2116-M-008-017, 108-2116-M-008-008, 109-2116-M-008-023 and 110-2116-M-008-004.

References

Auffret, Y., Pelleau, P., Klingelhoefer, F., Geli, L., Crozon, J., Lin, J.-Y., Sibuet, J.-C., 2004. MicrOBS: a new generation of ocean bottom seismometer. First Break 22, 41–47.
Becker, D., Meier, T., Rische, M., Bohnhoff, M., Harjes, H.-P., 2006. Spatio-temporal microseismicity clustering in the Cretan region. Tectonophysics 423, 3–16.
Briais, A., Patriat, P., Tapponnier, P., 1993. Updated interpretation of magnetic anomalies and seafloor spreading stages in the South China Sea: Implications for the Tertiary tectonics of Southeast Asia. J. Geophys. Res. Solid Earth 98, 6299–6328.
Chang, J.-H., Yu, H.-S., Lee, T.-Y., Hsu, H.-H., Liu, C.-S., Tsai, Y.-T., 2012. Characteristics of the outer rise seaward of the Manila Trench and implications in Taiwan–Luzon convergent belt, South China Sea. Mar. Geophys. Res. 33, 351–367.
Chin, S.-J., Lin, J.-Y., Yeh, Y.-C., Kuo-Chen, H., Liang, C.-W., 2019. Seismotectonic characteristics of the Taiwan collision-Manila subduction transition: the effect of pre-existing structures. J. Asian Earth Sci. 173, 113–120.
Christensen, D.H., Ruff, L.J., 1988. Seismic coupling and outer rise earthquakes. J. Geophys. Res. Solid Earth 93, 13421–13444.
Contreras-Reyes, E., Grevemeyer, I., Flueh, E.R., Scherwath, M., Heesemann, M., 2007. Alteration of the subducting oceanic lithosphere at the southern central Chile trench–outer rise. Geochem. Geophys. Geosyst. 8 (7) https://doi.org/10.1029/2007GC001632.
Craig, T., Copley, A., Jackson, J., 2014. A reassessment of outer rise seismicity and its implications for the mechanics of oceanic lithosphere. Geophys. J. Int. 197, 63–89.
Doo, W.B., Lo, C.L., Kuo-Chen, H., Brown, D., Hsu, S.K., 2015. Exhumation of serpentinized peridotite in the northern Manila subduction zone inferred from forward gravity modeling. Geophys. Res. Lett. 42, 7977–7982.
Eakin, D.H., McIntosh, K.D., Van Avendonk, H., Lavier, L., Lester, R., Liu, C.S., Lee, C.S., 2014. Crustal-scale seismic profiles across the Manila subduction zone: the transition from intraoceanic subduction to incipient collision. J. Geophys. Res. Solid Earth 119, 1–17.
Galgana, G., Hamburger, M., McCaffrey, R., Corpuz, E., Chen, Q., 2007. Analysis of crustal deformation in Luzon, Philippines using geodetic observations and earthquake focal mechanisms. Tectonophysics 432, 63–87.
Grevemeyer, I., Ranero, C.R., Flueh, E.R., Kläschen, D., Bialas, J., 2007. Passive and active seismological study of bending-related faulting and mantle serpentinization at the Middle America trench. Earth Planet. Sci. Lett. 258 (3–4), 528–542.
Hsu, S.-K., Yeh, Y.-c., Doo, W.-B., Tsai, C.-H., 2004. New bathymetry and magnetic lineations identifications in the northernmost South China Sea and their tectonic implications. Mar. Geophys. Res. 25, 29–44.
Hsu, Y.-J., Yu, S.-B., Simons, M., Kuo, L.-C., Chen, H.-Y., 2009. Interseismic crustal deformation in the Taiwan plate boundary zone revealed by GPS observations, seismicity, and earthquake focal mechanisms. Tectonophysics 479, 4–18.
Ivandic, M., Grevemeyer, I., Bialas, J., Petersen, C.J., 2010. Serpentinization in the trench-outer rise region offshore of Nicaragua: constraints from seismic refraction and wide-angle data. Geophys. J. Int. 180 (3), 1253–1264.
Kennett, B., Engdahl, E., 1991. Traveltimes for global earthquake location and phase identification. Geophys. J. Int. 105, 429–465.
Korenaga, J., 2017. On the extent of mantle hydration caused by plate bending. Earth Planet. Sci. Lett. 457, 1–9.
Ku, C.-Y., Hsu, S.-K., 2009. Crustal structure and deformation at the northern Manila Trench between Taiwan and Luzon islands. Tectonophysics 466, 229–240.
Lallemand, S., Peyret, M., van Rijsingen, E., Arcay, D., Heuret, A., 2018. Roughness characteristics of oceanic seafloor prior to subduction in relation to the seismogenic potential of subduction zones. Geochem. Geophys. Geosyst. 19 (7), 2121–2146.

Lester, R., McIntosh, K., Van Avendonk, H.J., Lavier, L., Liu, C.-S., Wang, T.-K., 2013. Crustal accretion in the Manila trench accretionary wedge at the transition from subduction to mountain-building in Taiwan. Earth Planet. Sci. Lett. 375, 430–440.
Lester, R., Van Avendonk, H.J., McIntosh, K., Lavier, L., Liu, C.S., Wang, T.K., Wu, F., 2014. Rifting and magmatism in the northeastern South China Sea from wide-angle tomography and seismic reflection imaging. J. Geophys. Res. Solid Earth 11 (3), 2305–2323. https://doi.org/10.1002/2013JB010639.
Liao, Y.-C., Hsu, S.-K., Chang, C.-H., Doo, W.-B., Ho, M.-Y., Lo, C.-L., Lee, C.-S., 2008. Seismic tomography off SW Taiwan: a joint inversion from OBS and onshore data of 2006 pingtung aftershocks. Terr. Atmos. Ocean. Sci. 19.
Lin, A.T., Yao, B., Hsu, S.-K., Liu, C.-S., Huang, C.-Y., 2009. Tectonic features of the incipient arc-continent collision zone of Taiwan: Implications for seismicity. Tectonophysics 479, 28–42.
Lin, J., Wu, W., Lo, C., 2015. Megathrust earthquake potential of the Manila subduction system: revealed by the seismic moment tensor element Mrr. Terr. Atmos. Ocean. Sci. 26, 619–630.
Lo, C.-L., Doo, W.-B., Kuo-Chen, H., Hsu, S.-K., 2017. Plate coupling across the northern Manila subduction zone deduced from mantle lithosphere buoyancy. Phys. Earth Planet. Inter. 273, 50–54.
McIntosh, K., van Avendonk, H., Lavier, L., Lester, W.R., Eakin, D., Wu, F., Liu, C.-S., Lee, C.-S., 2013. Inversion of a hyper-extended rifted margin in the southern Central Range of Taiwan. Geology 41, 871–874.
Naif, S., Key, K., Constable, S., Evans, R.L., 2015. Water-rich bending faults at the M iddle A merica T rench. Geochem. Geophys. Geosyst. 16 (8), 2582–2597.
Peacock, S.M., 2001. Are the lower planes of double seismic zones caused by serpentine dehydration in subducting oceanic mantle? Geology 29 (4), 299–302.
Qiu, Q., Li, L., Hsu, Y.-J., Wang, Y., Chan, C.-H., Switzer, A.D., 2019. Revised earthquake sources along Manila trench for tsunami hazard assessment in the South China Sea. Nat. Hazards Earth Syst. Sci. 19, 1565–1583.
Rangin, C., Le Pichon, X., Mazzotti, S., Pubellier, M., Chamot-Rooke, N., Aurelio, M., Walpersdorf, A., Quebral, R., 1999. Plate convergence measured by GPS across the Sundaland/Philippine Sea Plate deformed boundary: the Philippines and eastern Indonesia. Geophys. J. Int. 139, 296–316.
Seno, T., Stein, S., Gripp, A.E., 1993. A model for the motion of the Philippine Sea Plate consistent with NUVEL-1 and geological data. J. Geophys. Res. 98, 17941. https://doi.org/10.1029/93jb00782.
Sibuet, J.-C., Hsu, S.-K., Le Pichon, X., Le Formal, J.-P., Reed, D., Moore, G., Liu, C.-S., 2002. East Asia plate tectonics since 15 Ma: constraints from the Taiwan region. Tectonophysics 344, 103–134.
Tan, E., 2020. Subduction of transitional crust at the Manila Trench and its geophysical implications. J. Asian Earth Sci. 187, 104100.
Thurber, C.H., 1983. Earthquake locations and three-dimensional crustal structure in the Coyote Lake area, Central California. J. Geophys. Res. Solid Earth 88, 8226–8236.
Tilmann, F.J., Grevemeyer, I., Flueh, E.R., Dahm, T., Goßler, J., 2008. Seismicity in the outer rise offshore southern Chile: indication of fluid effects in crust and mantle. Earth Planet. Sci. Lett. 269, 41–55.
Trnkoczy, A., 2009. Understanding and Parameter Setting of STA/LTA Trigger Algorithm. New Manual of Seismological Observatory Practice (NMSOP), Deutsches GeoForschungsZentrum GFZ, pp. 1–20.
Tsai, C.H., Hsu, S.K., Yeh, Y.C., Lee, C.S., Xia, K., 2004. Crustal thinning of the northern continental margin of the South China Sea. Mar. Geophys. Res. 25 (1–2), 63–78. https://doi.org/10.1007/s11001-005-0733-5.
van Avendonk, H.J., Holbrook, W.S., Lizarralde, D., Denyer, P., 2011. Structure and serpentinization of the subducting Cocos plate offshore Nicaragua and Costa Rica. Geochem. Geophys. Geosyst. 12 (6) https://doi.org/10.1029/2011GC003592.
Wang, T.K., Chen, M.K., Lee, C.S., Xia, K., 2006. Seismic imaging of the transitional crust across the northeastern margin of the South China Sea. Tectonophysics 412 (3–4), 237–254. https://doi.org/10.1016/j.tecto.2005.10.039.
Watts, A.B., Talwani, M., 1974. Gravity anomalies seaward of deep-sea trenches and their tectonic implications. Geophys. J. Int. 36 (1), 57–90.
Wu, Y.-M., Zhao, L., Chang, C.-H., Hsiao, N.-C., Chen, Y.-G., Hsu, S.-K., 2009. Relocation of the 2006 Pingtung earthquake sequence and seismotectonics in Southern Taiwan. Tectonophysics 479, 19–27.
Wu, W.N., Kao, H., Hsu, S.K., Lo, C.L., Chen, H.W., 2010. Spatial variation of the crustal stress field along the Ryukyu-Taiwan-Luzon convergent boundary. J. Geophys. Res. Solid Earth 115.
Wu, W.N., Lo, C.L., Doo, W.-B., Lin, J.-Y., Hsu, S.-K., 2021. Seismogenic structure along the deformation front off SW Taiwan revealed by the aftershocks of the 2017 Tainan near-shore earthquake with ocean bottom seismometers. Tectonophysics 228995.
Yamashita, T., 1999. Pore Creation Due to Fault Slip in a Fluid-Permeated Fault Zone and its Effect on Seismicity: Generation Mechanism of Earthquake Swarm. Seismicity Patterns, Their Statistical Significance and Physical Meaning. Springer, pp. 625–647.
Yeh, Y.-C., Hsu, S.-K., 2004. Crustal structures of the northernmost South China Sea: Seismic reflection and gravity modeling. Mar. Geophys. Res. 25, 45–61.
Yeh, Y.C., Sibuet, J.C., Hsu, S.K., Liu, C.S., 2010. Tectonic evolution of the Northeastern South China Sea from seismic interpretation. J. Geophys. Res. Solid Earth 115.
Yeh, Y.-C., Hsu, S.-K., Doo, W.-B., Sibuet, J.-C., Liu, C.-S., Lee, C.-S., 2012. Crustal features of the northeastern South China Sea: insights from seismic and magnetic interpretations. Mar. Geophys. Res. 33, 307–326.
Yu, S.-B., Chen, H.-Y., Kuo, L.-C., 1997. Velocity field of GPS stations in the Taiwan area. Tectonophysics 274, 41–59.